

Strongly Entangled Kondo and Kagome Lattices and the Emergent Magnetic Ground State in Heavy-Fermion Kagome Metal YbV_6Sn_6

Rui Lou,^{1,2,3,*} Max Mende,⁴ Riccardo Vocaturo,¹ Hao Zhang,⁵ Qingxin Dong,^{6,7} Man Li,^{8,†} Pengfei Ding,⁹ Erjian Cheng,^{10,‡} Zhiguang Liao,⁹ Yu Zhang,⁹ Junfa Lin,⁹ Reza Firouzmandi,¹ Vilmos Kocsis,¹ Laura T. Corredor,¹ Yuri Prots,¹⁰ Oleksandr Suvorov,¹ Anupam Jana,^{11,12} Jun Fujii,¹¹ Ivana Vobornik,¹¹ Oleg Janson,¹ Wenliang Zhu,^{5,§} Jeroen van den Brink,^{1,13} Cornelius Krellner,¹⁴ Minghu Pan,^{5,15} Bosen Wang,^{6,7} Tianlong Xia,⁹ Jinguang Cheng,^{6,7} Shancai Wang,⁹ Claudia Felser,¹⁰ Bernd Büchner,^{1,4} Sergey Borisenko,¹ Rong Yu,⁹ Denis V. Vyalikh,^{16,17,¶} and Alexander Fedorov^{1,2,3,**}

¹Leibniz Institute for Solid State and Materials Research, IFW Dresden, 01069 Dresden, Germany

²Helmholtz-Zentrum Berlin für Materialien und Energie, Albert-Einstein-Straße 15, 12489 Berlin, Germany

³Joint Laboratory “Functional Quantum Materials” at BESSY II, 12489 Berlin, Germany

⁴Institut für Festkörper- und Materialphysik, Technische Universität Dresden, 01069 Dresden, Germany

⁵School of Physics and Information Technology, Shaanxi Normal University, Xi'an 710119, China

⁶Beijing National Laboratory for Condensed Matter Physics and Institute of Physics, Chinese Academy of Sciences, Beijing 100190, China

⁷School of Physical Sciences, University of Chinese Academy of Sciences, Beijing 100190, China

⁸School of Information Network Security, People's Public Security University of China, Beijing 100038, China

⁹School of Physics, Key Laboratory of Quantum State Construction and Manipulation (Ministry of Education), and Beijing Key Laboratory of Opto-Electronic Functional Materials & Micronano Devices, Renmin University of China, Beijing 100872, China

¹⁰Max Planck Institute for Chemical Physics of Solids, 01187 Dresden, Germany

¹¹CNR-IOM Istituto Officina dei Materiali, Area Science Park, 34149 Trieste, Italy

¹²International Centre for Theoretical Physics (ICTP), Str. Costiera 11, 34151 Trieste, Italy

¹³Institute for Theoretical Physics and Würzburg-Dresden Cluster of Excellence ct.qmat, Technische Universität Dresden, 01069 Dresden, Germany

¹⁴Kristall- und Materiallabor, Physikalisches Institut, Goethe-Universität Frankfurt, Max-von-Laue Strasse 1, 60438 Frankfurt am Main, Germany

¹⁵School of Physics, Huazhong University of Science and Technology, Wuhan 430074, China

¹⁶Donostia International Physics Center (DIPC), 20018 Donostia-San Sebastián, Spain

¹⁷IKERBASQUE, Basque Foundation for Science, 48011 Bilbao, Spain

Applying angle-resolved photoemission spectroscopy and density functional theory calculations, we present compelling spectroscopic evidence demonstrating the intertwining and mutual interaction between the Kondo and kagome sublattices in heavy-fermion intermetallic compound YbV_6Sn_6 . We reveal the Yb 4*f*-derived states near the Fermi level, along with the presence of bulk kagome bands and topological surface states. We unveil strong interactions between the 4*f* and itinerant electrons, where the kagome bands hosting the Dirac fermions and van Hove singularities predominate. Such findings are well described using a *c-f* hybridization model. On the other hand, our systematic characterization of magnetic properties demonstrates an unusually enhanced antiferromagnetic ordering, where the kagome-derived van Hove singularities near E_F play a vital role in determining the unconventional nature of the Ruderman-Kittel-Kasuya-Yosida interaction and Kondo coupling. These unique kagome-state-mediated exchange interactions have never been reported before and could lead to a novel phase diagram and various quantum critical behaviors in YbV_6Sn_6 and its siblings. Our results not only expand the family of exotic quantum phases entangled with kagome structure to the strongly correlated regime, but also establish YbV_6Sn_6 as an unprecedented platform to explore unconventional many-body physics beyond the standard Kondo picture.

Exploring the mutual interactions among correlated states, magnetism, and topological phenomena is at the forefront of condensed-matter research [1–6]. Kagome lattices are emerging platforms for studying this entanglement. A variety of electronic instabilities and nontrivial band topologies, such as Chern-gapped Dirac fermion [7, 8], charge density wave [9–12], nematicity [13, 14], superconductivity [10–13], and pair density wave [15] have been observed. Due to the unique lattice geometry, three typical band features are identified, including the flat band (FB), Dirac point (DP), and van Hove singularities (vHSs) [16]. The essential role of kagome band structure in the formation of these symmetry-breaking states has been extensively studied [17–24].

The discovery of heavy-fermion compound YbV_6Sn_6 of-

fers a precious opportunity to study kagome physics in the presence of strongly correlated 4*f* states [25]. In the framework of the Kondo effect, when the *f* electrons are arranged in a Kondo lattice, the strong interactions between itinerant conduction electrons and localized *f* electrons lead to band reconstructions and opening of hybridization gaps, namely, the *c-f* hybridization [26–28]. This gives rise to strongly renormalized quasiparticles with huge effective masses, called heavy fermions [29, 30]. Despite the tremendous efforts devoted to other intermetallic RV_6Sn_6 ($R = \text{Y, Gd-Tm, Lu}$) [31–35], the interplay of the correlation effects from the rare-earth sublattice and those associated with the exotic electronic states of V-based kagome network remains unexplored. With the adjacent triangular Kondo lattice and kagome lattice layers,

YbV_6Sn_6 provides a unique platform to study the interplay between strong $4f$ electronic correlations and kagome band structures. It is therefore desirable to explore spectroscopic evidence for these two sublattices and their potential coupling.

In parallel, an antiferromagnetic ordering was observed in YbV_6Sn_6 below ~ 0.4 K, and its suppression by a weak magnetic field induces the non-Fermi-liquid behavior [25], signifying the proximity of YbV_6Sn_6 to a potential quantum critical point (QCP). Further delving into the origin of magnetic ground state would shed light on the quantum criticality in a kagome metal, which still remains largely unknown.

By employing angle-resolved photoemission spectroscopy (ARPES) and density functional theory (DFT) calculations, here we uncover the entanglement of Kondo and kagome sublattices in YbV_6Sn_6 —the strong hybridizations between Yb $4f$ states close to E_F and kagome bands constituting the DPs and vHSs. Intriguingly, an unexpected enhancement of the antiferromagnetic order is observed. We suggest that the unconventional nature of the underlying Ruderman-Kittel-Kasuya-Yosida (RKKY) and Kondo interactions originates from their being mediated primarily by the kagome electrons, where the enhanced density of states (DOS) and electron correlations associated with vHSs play a crucial role.

High-quality YbV_6Sn_6 single crystals were grown by the self-flux method [25, 36]. YbV_6Sn_6 crystallizes in a $P6/mmm$ HfFe_6Ge_6 -type structure [56], featuring the Yb-based triangular and V-based kagome sublattices [Figs. 1(a) and 1(b)]. The bulk and (001)-projected surface Brillouin zones (BZs) are depicted in Fig. 1(c). The occurrence of intermediate valence in rare-earth intermetallic materials has been suggested as characteristic of the Kondo effect [57]. To examine the $4f$ occupation in YbV_6Sn_6 , we measure the temperature-dependent

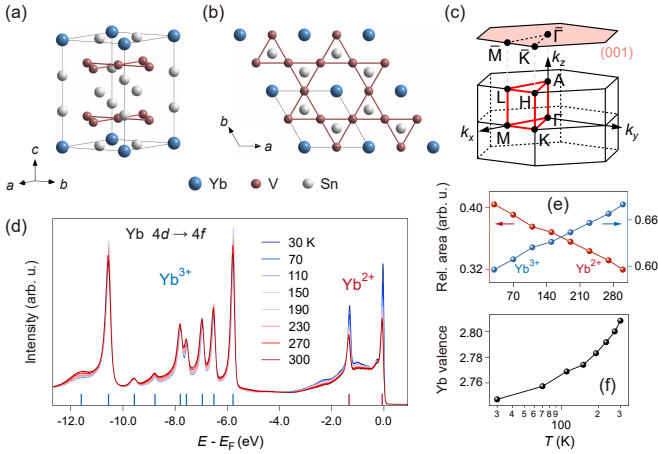


FIG. 1: (a),(b) Side and top views of the YbV_6Sn_6 crystal structure, respectively. (c) Bulk and (001)-projected surface BZs. (d) Temperature-dependent angle-integrated photoemission intensity ($h\nu = 182$ eV). The Yb^{2+} and Yb^{3+} components are marked out by the red and blue bars, respectively. (e) Temperature-dependent relative peak areas of Yb^{2+} and Yb^{3+} features. Before the normalization, a Shirley-type background has been subtracted from both components. (f) Temperature dependence of the estimated Yb valence.

angle-integrated photoemission spectra on the Sn termination [Fig. 1(d)]. Under the Yb $4d \rightarrow 4f$ resonant photon energy [58], we reveal the Yb^{2+} ($4f^{14} \rightarrow 4f^{13}$ transition) and Yb^{3+} ($4f^{13} \rightarrow 4f^{12}$ transition) components, manifesting as doublet ($4f_{7/2}$ and $4f_{5/2}$) and multiplet, respectively. The extracted relative peak areas of Yb^{2+} and Yb^{3+} features clearly show the temperature evolution of $4f$ occupation, as presented in Fig. 1(e). Accordingly, the Yb valence can be estimated [Fig. 1(f), see estimation process and more discussion in Sec. 2 of Supplemental Material (SM)]. Their temperature dependences are similar to other Yb-based heavy-fermion and valence-fluctuating systems, like YbRh_2Si_2 [59], YbInCu_4 [60, 61], and YbAl_3 [62]. The Kondo lattice behavior of YbV_6Sn_6 is also embodied in electrical resistivity measurements (Fig. S1), where the zero-field $\rho(T)$ resembles that of many other heavy-fermion compounds [63–65].

To characterize the typical electronic structures of kagome [Fig. S2(a)] and Kondo [Fig. S2(b)] sublattices as well as their underlying interactions, we conduct ARPES experiments on YbV_6Sn_6 . Based on the line shape of Sn $4d$ core levels [66] and no evident Yb $4f$ surface signals [67] in our measurements, we obtained two surface terminations upon cleaving (V_3Sn and Sn). The corresponding band structures are shown in Figs. 2 and S3. Similar to GdV_6Sn_6 [68] and TbV_6Sn_6 [69], the Sn termination shows Sn $4d$ core levels from both bulk and surface Sn atoms [Fig. S3(a)], while the V_3Sn termination only shows the signals from bulk Sn atoms [Fig. 2(a)]. Although the ARPES mappings from Sn termination exhibit richer topologies [Figs. S3(b)-S3(d)] compared to V_3Sn termination [Figs. 2(b)-2(d)], the typical features of a kagome lattice, the corner-sharing triangular pockets centered at \bar{K} [22], are recognized on both terminations.

Figures 2(e) and S3(e) show the ARPES spectra along the $\bar{\Gamma}-\bar{M}-\bar{\Gamma}$ directions, two shallow electron bands are observed in

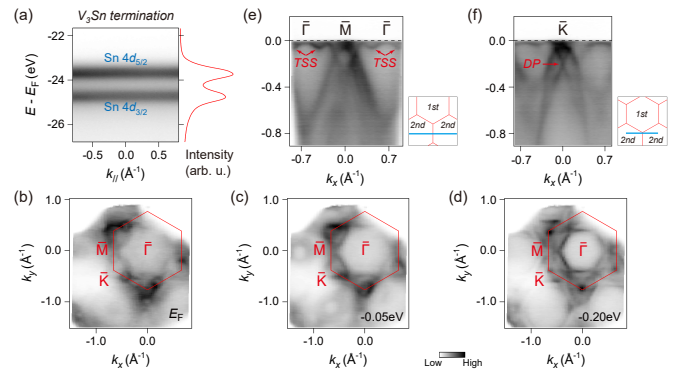


FIG. 2: (a) X-ray photoelectron spectroscopy spectrum ($h\nu = 100$ eV) (left) and corresponding integrated energy distribution curve (right) measured on the V_3Sn termination. (b)-(d) Constant-energy ARPES images [$h\nu = 80$ eV, linear horizontal (LH) polarization] from the V_3Sn termination at the energies of 0, -0.05, and -0.20 eV, respectively. (e),(f) Corresponding ARPES intensity plots ($T \approx 2$ K) around \bar{M} and \bar{K} , respectively. The momentum locations are illustrated in the insets. The 50-eV photons were used to better reveal the TSSs and DP.

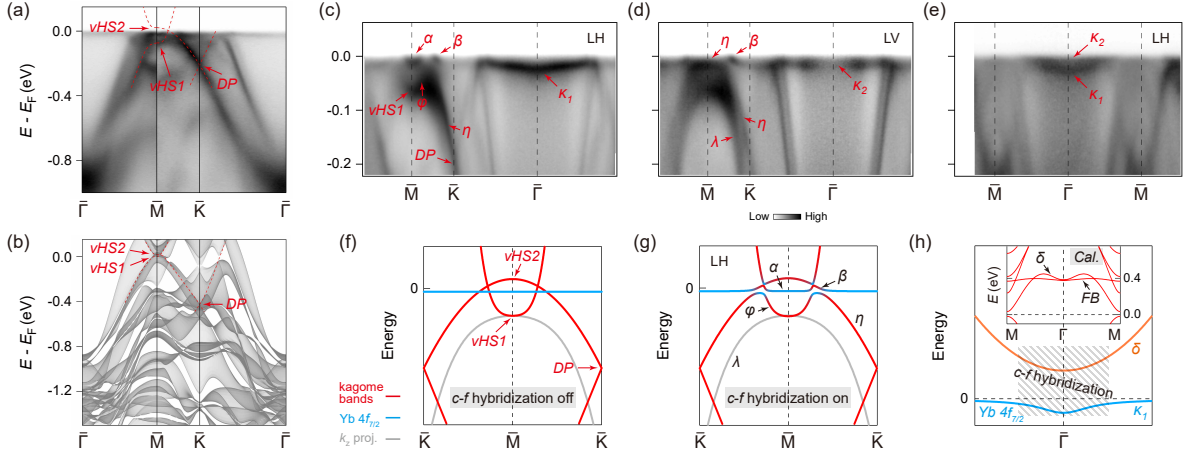


FIG. 3: (a) Experimental band structures of YbV_6Sn_6 along the $\bar{\Gamma}\text{-}\bar{M}\text{-}\bar{K}\text{-}\bar{\Gamma}$ lines at 2 K. The typical kagome bands are guided by the red dashed curves (without including the effect of c - f hybridization). (b) DFT calculated bulk bands with the integration over entire k_z . The contribution of the Yb $4f$ shell is not included. (c),(d) ARPES intensity plots along the $\bar{\Gamma}\text{-}\bar{K}\text{-}\bar{M}$ directions at 2 K recorded by 53-eV photons with LH and LV polarizations, respectively. (e) Same as (c) along the $\bar{\Gamma}\text{-}\bar{M}$ direction. (f),(g) Schematic band diagrams along the $\bar{K}\text{-}\bar{M}\text{-}\bar{K}$ directions without and with considering the c - f hybridization, respectively. A simple band hybridization model is constructed. (h) Sketches of the hybridization between δ band and $4f_{7/2}^{13}$ state at $\bar{\Gamma}$. Inset: Calculated bulk bands along the $M\text{-}\Gamma\text{-}M$ direction.

the second BZ for both terminations, where the intensity on the Sn termination is intrinsically weak (more pronounced) at higher (lower) photon energies due to the k_z selection rules (Fig. S4). These bands resemble the topological surface states (TSSs) in GdV_6Sn_6 [70] (see Fig. S5 and Sec. 3 of SM for the slab calculations and more discussion). We further measure the band dispersions near \bar{K} . As shown in Figs. 2(f) and S3(f), the linear bands cross each other at about -0.2 eV to form the kagome DP at \bar{K} . Such bulk kagome bands are native to the kagome lattice irrespective of surface termination. Below we focus on the intrinsic bulk kagome band structures.

Figure 3(a) summarizes the experimental band dispersions along the $\bar{\Gamma}\text{-}\bar{M}\text{-}\bar{K}\text{-}\bar{\Gamma}$ lines. By comparing with the DFT calculations [Figs. 3(b) and S6], we obtain a good overall agreement and experimentally identify the typical band structure of the kagome sublattice. Specifically, the vHS1 is observed at about -0.07 eV at \bar{M} ; the DP at about -0.2 eV is revealed around \bar{K} ; the upper branch of the DP disperses up to constitute the vHS2 slightly above E_F at \bar{M} . Similar kagome bands near E_F have also been identified in GdV_6Sn_6 [70] and TbV_6Sn_6 [33].

We now proceed to explore the ARPES signatures of the Kondo sublattice and its potential intertwining with the kagome sublattice. As shown in Fig. 3(c) (LH polarization), the bulk kagome bands identified before exhibit appreciable discontinuity when approaching the Yb $4f_{7/2}^{13}$ states close to E_F , in sharp contrast to other RV_6Sn_6 compounds without $4f$ levels near E_F , like GdV_6Sn_6 [68, 70], TbV_6Sn_6 [33], and HoV_6Sn_6 [68]. The electron-like vHS1 band (φ) and the Dirac band (η) bend back to merge with each other below E_F [see Figs. S7(b)(i),(c)(i) and S8(b)(i),(c)(i) under other photon energies]. A depletion of intensity is observed between the φ/η band top and the two shallow bands (α and β), pointing to the opening of energy gaps. These facts suggest the presence of

hybridizations between kagome bands and $4f$ states, which can be well accounted for by the c - f hybridization model [27, 28]. As illustrated in Fig. 3(f), we sketch the original features along the $\bar{K}\text{-}\bar{M}\text{-}\bar{K}$ line before the hybridization. It is seen that both the vHS1 band and Dirac band (or vHS2 band) will interact with the dispersionless $4f_{7/2}^{13}$ state. When the c - f hybridization is included [Fig. 3(g)], hybridization gaps open at the intersections. Specifically, the $4f$ -derived states disperse upward and merge with the upper unhybridized parts of kagome bands; the $4f$ level merged with the vHS1 band further interacts with the vHS2 band slightly above E_F , leading to the α and β bands; the lower unhybridized kagome bands bend back to form the φ/η band top with strong $4f$ admixtures [also see band structure cartoon in Fig. S9(b)]. The validity of this model is further corroborated by our Cs-dosing experiments (Fig. S10). Systematic temperature-dependent measurements (Fig. S11) demonstrate that such hybridizations occur already at high temperatures (see detailed discussion in Sec. 5 of SM).

We then record the ARPES spectra with linear vertical (LV) polarization. In Fig. 3(d), one sees that the β band remains while the α and φ bands are not present, in addition, the η band disperses towards E_F till being flattened around \bar{M} [see Figs. S7(b)(ii),(c)(ii) and S8(b)(ii),(c)(ii) under other photon energies]. Accordingly, a gap opens between the β and η bands. With the three-dimensionality of the electronic structure revealed by photon-energy-dependent measurements (Fig. S12), the vHS1 band (along $\bar{K}\text{-}\bar{M}\text{-}\bar{K}$ direction) would lie completely above the $4f_{7/2}^{13}$ state in certain k_z planes, as seen in Figs. 3(b) and S6. The projection from such k_z 's coexists with the one from $k_z = 0$ due to the k_z -broadening effect [71]. Whereas, these two sets of k_z -projected vHS1 bands most likely have different orbital characters [72], making themselves separately visible under different photon po-

larizations (see Table S1 and Sec. 7 of SM for the matrix element analysis). In the case of LV polarization, as illustrated in Fig. S9(c), only the vHS2 band will interact with the $4f$ state, resulting in the observations in Fig. 3(d).

Next, we turn to the band structure around $\bar{\Gamma}$. In Fig. 3(c), the $4f_{7/2}^{13}$ state (κ_1) is pushed slightly downwards at $\bar{\Gamma}$ (see Fig. S12 for its bulk origin). Similar phenomenon has been observed before in YbRh_2Si_2 and suggested to originate from the interactions between the $4f$ states and an unoccupied electron band [27]. Such hybridization can be described by the periodic Anderson model calculations [67] and has been evidenced by the extended quasiparticle lifetimes of the involved unoccupied states in time-resolved ARPES measurements of YbRh_2Si_2 [73]. In our case, as suggested by the calculations [inset of Fig. 3(h) and S6], the corresponding unoccupied band could be the parabolic band (δ) whose bottom degenerates with the kagome FB at ~ 0.37 eV. Figure 3(h) depicts the hybridization between δ band and $4f_{7/2}^{13}$ state, which is another indicator of the intertwined Kondo and kagome sublattices, because the δ extends to form the kagome band features at M and K (Fig. S6). Upon switching to LV polarization [Fig. 3(d)], instead of κ_1 , a flat $4f$ state (κ_2) without hybridization is revealed at $\bar{\Gamma}$ [also see Fig. S8(a)(ii)]. These results taken together indicate the presence of two split $4f_{7/2}^{13}$ states around $\bar{\Gamma}$. This is further underpinned by the spectra along the $\bar{\Gamma}$ - \bar{M} direction [Fig. 3(e)], where the two split states are simultaneously detected (see Figs. S7 and S8 for more data). Such observations provide direct evidence that the $4f_{7/2}^{13}$ state undergoes the crystalline electric field splitting [74] whose energy scale at BZ center is of ~ 20 meV, which is comparable to the typical order of magnitude for crystalline electric field effects in $4f$ -based systems [27].

A recent study proposed that YbV_6Sn_6 is near a potential antiferromagnetic QCP [25]. To gain insights into the magnetic ground state, we perform low-temperature heat capacity, magnetization, and electrical resistivity measurements. As presented in Fig. 4(a), the zero-field C_p/T of our samples follows similar Fermi-liquid behavior as in Ref. [25] from ~ 4 to 10 K, showing a comparable Sommerfeld coefficient ($\gamma \sim 383$ mJ/mol K²). Interestingly, a pronounced increase below ~ 4 K followed by a peak formation at ~ 2.2 K are observed. The λ -shaped peak at ~ 2.2 K in C_p [Fig. 4(b)] indicates a second-order phase transition. The evolution of this peak under the magnetic field [Fig. 4(c)] is similar to that of the 0.4-K peak in Ref. [25]. Further, our magnetization [Fig. 4(d)] and electrical resistivity [Fig. 4(e) and Sec. 9 of SM] measurements confirm that the nature of this transition is indeed an antiferromagnetically ordered state. These observations demonstrate that the previously reported antiferromagnetism has been notably enhanced in our sample (labeled as YVS22).

The proximity to QCP renders the antiferromagnetic order sensitive to the extrinsic parameters like pressure, magnetic field, or chemical substitution [75]. Given the observed lattice expansion in YVS22 (see Fig. S15 for the x-ray diffraction data) compared to Guo *et al.*'s [25], it is inferred that the revealed enhancement could arise from the negative chemi-

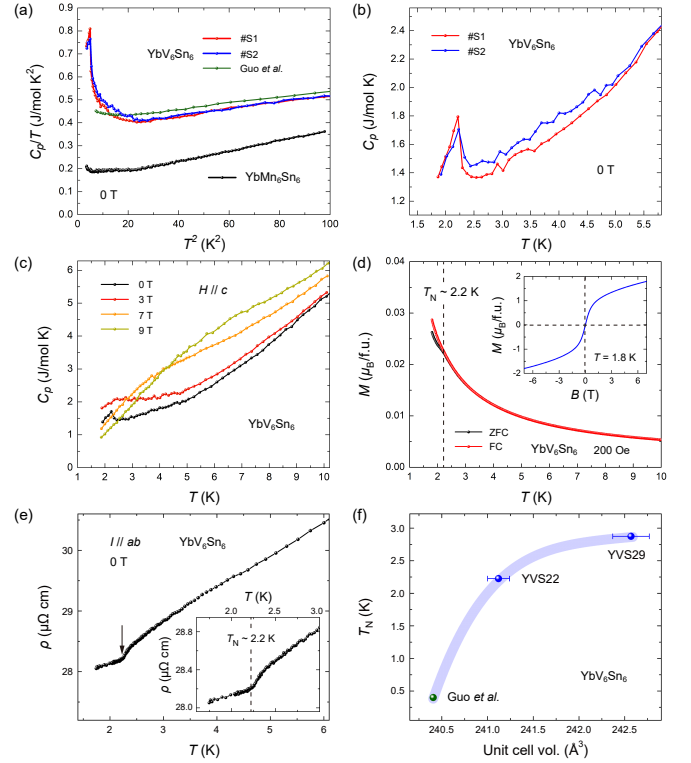


FIG. 4: (a) Zero-field specific heat of YbV_6Sn_6 and YbMn_6Sn_6 plotted as C_p/T vs T^2 . The green curve is adopted from Ref. [25]. (b) Low-temperature specific heat of YbV_6Sn_6 in zero field. (c) Temperature-dependent specific heat of YbV_6Sn_6 in different magnetic fields ($H \parallel c$). (d) Temperature dependence of zero-field-cooling and field-cooling magnetization of YbV_6Sn_6 ($H \parallel ab$). Inset: Field-dependent magnetization at 1.8 K ($H \parallel ab$). (e) Temperature-dependent zero-field resistivity of YbV_6Sn_6 ($I \parallel ab$). Inset shows temperature range close to T_N . (f) T_N of YbV_6Sn_6 as a function of unit cell volume. The green dot is adopted from Ref. [25].

cal pressure effect. To investigate whether T_N can be further increased, we have slightly modified the growth conditions. It turns out that slightly elevated growth temperatures result in an increase of T_N to ~ 2.9 K [Fig. S16(a), labeled as YVS29]. Meanwhile, the lattice of YVS29 (Table S2) is further expanded compared to YVS22. Accordingly, the variation of T_N with the unit cell volume is summarized in Fig. 4(f). Although the origin of the lattice expansion remains unclear and warrants further investigation, the present results indicate an intrinsic link between antiferromagnetic order and lattice parameters. Furthermore, our high-pressure studies of YVS29 reveal that the antiferromagnetic order is progressively weakened with increasing hydrostatic pressure [Figs. S16(b)-S16(d)]. Taken together, these results demonstrate that the antiferromagnetism in YbV_6Sn_6 strengthens with lattice expansion and diminishes under lattice compression, establishing YbV_6Sn_6 as a compelling system for realizing a pressure-induced QCP. An alternative approach to accessing the QCP would be through fine-tuned Mn substitution on V sites, because the Mn sublattices order ferromagnetically while the Yb atoms have no magnetic moment in

YbMn₆Sn₆ [76, 77]. The obtained $\gamma \sim 144$ mJ/mol K² [Fig. 4(a)] and intermediate valence behavior (Fig. S17) evidence the presence of heavy-fermion state in YbMn₆Sn₆ (see more discussion in Sec. 12 of SM). Our findings establish a robust heavy-fermion kagome system irrespective of the rich magnetic ground states.

In a Kondo lattice system, the magnetic ground state is determined by the competition between RKKY and Kondo interactions, whose energy scales are characterized by $T_{\text{RKKY}} \propto J^2 g(E_F)$ and $T_K \propto \exp(-1/Jg(E_F))$, respectively, where $g(E_F)$ is the conduction-band DOS at E_F and $J \propto V^2/(E_F - E_f)$ is the magnetic exchange coupling between conduction electrons and f electrons, depending on the c - f hybridization (V) and the energy location of f level (E_f). According to the Doniach diagram [78], YbV₆Sn₆ is situated in the intermediate J regime. In a conventional Kondo picture, pressurizing such Yb-based compounds would suppress the valence fluctuations and readily drive the system towards the $4f^{13}$ configuration, resulting in more localized $4f$ states and weaker J [79]. Consequently, T_{RKKY} and T_K decrease with increasing positive pressure, and T_N would first increase and then decrease. Accordingly, the negative pressure would enhance J , and the increasingly screened magnetic moments would lead to the decrease of T_N . However, this conventional Kondo paradigm fails to account for our observations, indicating an exotic origin. In Fig. S19, our DFT calculations reveal that the vHS1 and vHS2 remain close to E_F under various hydrostatic pressures, giving rise to a large DOS around E_F and enhanced many-body interactions, which imply that much more conduction states are involved in the c - f hybridization in YbV₆Sn₆ compared to other systems. These abundant kagome electron channels can promote the valence fluctuations and stabilize the intermediate valence states. Thereby, the Yb valence would evolve smoothly and slowly under pressure, rendering the pressure dependence of J predominantly governed by V . In this context, J would be enhanced (weakened) by the lattice compression (lattice expansion) due to the increased (reduced) overlap between the wavefunctions of conduction states and f states. Thus, T_{RKKY} and T_K of YbV₆Sn₆ would increase (decrease) with increasing positive pressure (negative pressure), and the increasingly (less) screened magnetic moments result in the decrease (increase) of T_N (see more detailed discussion in Sec. 13 of SM). Such kagome-state-mediated RKKY and Kondo interactions, intertwined with the geometric frustration, underpin a landscape of unconventional many-body physics beyond the standard Kondo framework.

In summary, we have revealed a strong entanglement between the Kondo and kagome sublattices in YbV₆Sn₆. The unique kagome-mediated RKKY and Kondo interactions lead to an emergent antiferromagnetic ground state. Our results highlight YbV₆Sn₆ as a promising system that can exhibit novel quantum criticality and richer Kondo physics.

We would like to thank Rui-Zhen Huang and Anmin Zhang for inspiring discussions. This work was supported by the Deutsche Forschungsgemeinschaft under Grant SFB 1143 (project C04), the Würzburg-Dresden Cluster of Excellence

on Complexity and Topology in Quantum Matter – *ct.qmat* (EXC 2147, project ID 390858490), the National Key R&D Program of China (Grants No. 2022YFA1403100 and No. 2022YFA1403101), the National Natural Science Foundation of China (Grants No. 12204297 and No. 12204536), the Fundamental Research Funds for the Central Universities, and the Research Funds of People's Public Security University of China (PPSUC) (2023JKF02ZK09). E. J. C. acknowledges the financial support from the Alexander von Humboldt Foundation. L. T. C. is funded by the DFG (project-id 456950766). B. B. and S. B. acknowledge the support from the BMBF via project UKRATOP. The high-pressure measurements were partially supported by the Cubic Anvil Cell station of Synergic Extreme Condition User Facility (SECUF).

* lourui09@gmail.com

† lmrucphys@ruc.edu.cn

‡ Erjian.Cheng@cpfs.mpg.de

§ wlzhu@snnu.edu.cn

¶ denis.vyalikh@dicp.org

** a.fedorov@ifw-dresden.de

- [1] Y. Deng, Y. Yu, M. Shi, Z. Guo, Z. Xu, J. Wang, X. Chen, and Y. Zhang, *Quantum anomalous Hall effect in intrinsic magnetic topological insulator MnBi₂Te₄*, Science **367**, 895 (2020).
- [2] M. Serlin, C. L. Tschirhart, H. Polshyn, Y. Zhang, J. Zhu, K. Watanabe, T. Taniguchi, L. Balents, and A. F. Young, *Intrinsic quantized anomalous Hall effect in a moiré heterostructure*, Science **367**, 900 (2020).
- [3] P. Zhang, K. Yaji, T. Hashimoto, Y. Ota, T. Kondo, K. Okazaki, Z. Wang, J. Wen, G. D. Gu, H. Ding, and S. Shin, *Observation of topological superconductivity on the surface of an iron-based superconductor*, Science **360**, 182 (2018).
- [4] S. Zhu, L. Kong, L. Cao, H. Chen, M. Papaj, S. Du, Y. Xing, W. Liu, D. Wang, C. Shen, F. Yang, J. Schneeloch, R. Zhong, G. D. Gu, L. Fu, Y. Zhang, H. Ding, and H.-J. Gao, *Nearly quantized conductance plateau of vortex zero mode in an iron-based superconductor*, Science **367**, 189 (2020).
- [5] Q. Gu, J. P. Carroll, S. Wang, S. Ran, C. Broyles, H. Siddiquee, N. P. Butch, S. R. Saha, J. Paglione, J. C. Séamus Davis, and X. Liu, *Detection of a pair density wave state in UTe₂*, Nature (London) **618**, 921 (2023).
- [6] Y. Liu, T. Wei, G. He, Y. Zhang, Z. Q. Wang, and J. Wang, *Pair density wave state in a monolayer high- T_c iron-based superconductor*, Nature (London) **618**, 934 (2023).
- [7] J.-X. Yin, W. Ma, T. A. Cochran, X. Xu, S. S. Zhang, H.-J. Tien, N. Shumiya, G. Cheng, K. Jiang, B. Lian, Z. Song, G. Chang, I. Belopolski, D. Multer, M. Litskevich, Z.-J. Cheng, X. P. Yang, B. Swidler, H. Zhou, H. Lin, T. Neupert, Z. Wang, N. Yao, T.-R. Chang, S. Jia, and M. Z. Hasan, *Quantum-limit Chern topological magnetism in TbMn₆Sn₆*, Nature (London) **583**, 533 (2020).
- [8] W. Ma, X. Xu, J. Yin, H. Yang, H. Zhou, Z. Cheng, Y. Huang, Z. Qu, F. Wang, M. Z. Hasan, and S. Jia, *Rare earth engineering in RMn₆Sn₆ ($R = \text{Gd-Tm, Lu}$) topological kagome magnets*, Phys. Rev. Lett. **126**, 246602 (2021).
- [9] B. R. Ortiz, L. C. Gomes, J. R. Morey, M. Winiarski, M. Bordelon, J. S. Mangum, I. W. H. Oswald, J. A. Rodriguez-Rivera, J. R. Neilson, S. D. Wilson, E. Ertekin, T. M. McQueen, and

- E. S. Toberer, *New kagome prototype materials: discovery of KV_3Sb_5 , RbV_3Sb_5 , and CsV_3Sb_5* , Phys. Rev. Mater. **3**, 094407 (2019).
- [10] B. R. Ortiz, S. M. L. Teicher, Y. Hu, J. L. Zuo, P. M. Sarte, E. C. Schueller, A. M. M. Abeykoon, M. J. Krogstad, S. Rosenkranz, R. Osborn, R. Seshadri, L. Balents, J. He, and S. D. Wilson, *CsV_3Sb_5 : a \mathbb{Z}_2 topological kagome metal with a superconducting ground state*, Phys. Rev. Lett. **125**, 247002 (2020).
- [11] Q. Yin, Z. Tu, C. Gong, Y. Fu, S. Yan, and H. C. Lei, *Superconductivity and normal-state properties of kagome metal RbV_3Sb_5 single crystals*, Chin. Phys. Lett. **38**, 037403 (2021).
- [12] B. R. Ortiz, P. M. Sarte, E. M. Kenney, M. J. Graf, S. M. L. Teicher, R. Seshadri, and S. D. Wilson, *Superconductivity in the \mathbb{Z}_2 kagome metal KV_3Sb_5* , Phys. Rev. Mater. **5**, 034801 (2021).
- [13] H. Yang, Y. Ye, Z. Zhao, J. Liu, X.-W. Yi, Y. Zhang, J. Shi, J. You, Z. Huang, B. Wang, J. Wang, H. Guo, X. Lin, C. Shen, W. Zhou, H. Chen, X. Dong, G. Su, Z. Q. Wang, and H.-J. Gao, *Superconductivity and orbital-selective nematic order in a new titanium-based kagome metal $CsTi_3Bi_5$* , arXiv:2211.12264.
- [14] H. Li, S. Y. Cheng, B. R. Ortiz, H. X. Tan, D. Werhahn, K. Y. Zeng, D. Johrendt, B. H. Yan, Z. Q. Wang, S. D. Wilson, and I. Zeljkovic, *Electronic nematicity without charge density waves in titanium-based kagome metal*, Nat. Phys. **19**, 1591 (2023).
- [15] H. Chen, H. Yang, B. Hu, Z. Zhao, J. Yuan, Y. Xing, G. Qian, Z. Huang, G. Li, Y. Ye, S. Ma, S. Ni, H. Zhang, Q. Yin, C. Gong, Z. Tu, H. C. Lei, H. Tan, S. Zhou, C. Shen, X. Dong, B. Yan, Z. Q. Wang, and H.-J. Gao, *Roton pair density wave in a strong-coupling kagome superconductor*, Nature (London) **599**, 222 (2021).
- [16] M. Li, Q. Wang, G. Wang, Z. Yuan, W. Song, R. Lou, Z. T. Liu, Y. Huang, Z. Liu, H. C. Lei, Z. P. Yin, and S.-C. Wang, *Dirac cone, flat band and saddle point in kagome magnet YMn_6Sn_6* , Nat. Commun. **12**, 3129 (2021).
- [17] J.-X. Yin, S. S. Zhang, G. Chang, Q. Wang, S. S. Tsirkin, Z. Guguchia, B. Lian, H. Zhou, K. Jiang, I. Belopolski, N. Shumiya, D. Multer, M. Litskevich, T. A. Cochran, H. Lin, Z. Q. Wang, T. Neupert, S. Jia, H. C. Lei, and M. Z. Hasan, *Negative flat band magnetism in a spin-orbit-coupled correlated kagome magnet*, Nat. Phys. **15**, 443 (2019).
- [18] H. Huang, L. Zheng, Z. Lin, X. Guo, S. Wang, S. Zhang, C. Zhang, Z. Sun, Z. Wang, H. Weng, L. Li, T. Wu, X. Chen, and C. G. Zeng, *Flat-band-induced anomalous anisotropic charge transport and orbital magnetism in kagome metal $CoSn$* , Phys. Rev. Lett. **128**, 096601 (2022).
- [19] H. X. Tan, Y. Liu, Z. Q. Wang, and B. H. Yan, *Charge density waves and electronic properties of superconducting kagome metals*, Phys. Rev. Lett. **127**, 046401 (2021).
- [20] M. M. Denner, R. Thomale, and T. Neupert, *Analysis of charge order in the kagome metal AV_3Sb_5 ($A = K, Rb, Cs$)*, Phys. Rev. Lett. **127**, 217601 (2021).
- [21] X. Zhou, Y. Li, X. Fan, J. Hao, Y. Dai, Z. Wang, Y. Yao, and H.-H. Wen, *Origin of charge density wave in the kagome metal CsV_3Sb_5 as revealed by optical spectroscopy*, Phys. Rev. B **104**, L041101 (2021).
- [22] R. Lou, A. Fedorov, Q. W. Yin, A. Kuibarov, Z. J. Tu, C. S. Gong, E. F. Schwier, B. Büchner, H. C. Lei, and S. Borisenko, *Charge-density-wave-induced peak-dip-hump structure and the multiband superconductivity in a kagome superconductor CsV_3Sb_5* , Phys. Rev. Lett. **128**, 036402 (2022).
- [23] X. Teng, J. S. Oh, H. Tan, L. Chen, J. Huang, B. Gao, J. Yin, J.-H. Chu, M. Hashimoto, D. Lu, C. Jozwiak, A. Bostwick, E. Rotenberg, G. E. Granroth, B. Yan, R. J. Birgeneau, P. C. Dai, and M. Yi, *Magnetism and charge density wave order in kagome $FeGe$* , Nat. Phys. **19**, 814 (2023).
- [24] Y. Luo, Y. Han, J. Liu, H. Chen, Z. Huang, L. Huai, H. Li, B. Wang, J. Shen, S. Ding, Z. Li, S. Peng, Z. Wei, Y. Miao, X. Sun, Z. Ou, Z. Xiang, M. Hashimoto, D. Lu, Y. G. Yao, H. Yang, X. Chen, H.-J. Gao, Z. Qiao, Z. Wang, and J. He, *A unique van Hove singularity in kagome superconductor $CsV_{3-x}Ta_xSb_5$ with enhanced superconductivity*, Nat. Commun. **14**, 3819 (2023).
- [25] K. Guo, J. Ye, S. Guan, and S. Jia, *Triangular Kondo lattice in YbV_6Sn_6 and its quantum critical behavior in a magnetic field*, Phys. Rev. B **107**, 205151 (2023).
- [26] P. Coleman, *Handbook of Magnetism and Advanced Magnetic Materials*, edited by H. Kronmüller and S. Parkin (John Wiley, New York, 2007), pp. 95–148.
- [27] D. V. Vyalikh, S. Danzenbächer, Y. Kucherenko, K. Kummer, C. Krellner, C. Geibel, M. G. Holder, T. K. Kim, C. Laubschat, M. Shi, L. Patthey, R. Follath, and S. L. Molodtsov, *k dependence of the crystal-field splittings of 4f states in rare-earth systems*, Phys. Rev. Lett. **105**, 237601 (2010).
- [28] S. Danzenbächer, D. V. Vyalikh, K. Kummer, C. Krellner, M. Holder, M. Höppner, Y. Kucherenko, C. Geibel, M. Shi, L. Patthey, S. L. Molodtsov, and C. Laubschat, *Insight into the f-derived Fermi surface of the heavy-fermion compound $YbRh_2Si_2$* , Phys. Rev. Lett. **107**, 267601 (2011).
- [29] G. R. Stewart, *Heavy-fermion systems*, Rev. Mod. Phys. **56**, 755 (1984).
- [30] G. R. Stewart, *Non-Fermi-liquid behavior in d- and f-electron metals*, Rev. Mod. Phys. **73**, 797 (2001).
- [31] G. Pokharel, S. M. L. Teicher, B. R. Ortiz, P. M. Sarte, G. Wu, S. Peng, J. He, R. Seshadri, and S. D. Wilson, *Electronic properties of the topological kagome metals YV_6Sn_6 and GdV_6Sn_6* , Phys. Rev. B **104**, 235139 (2021).
- [32] J. Lee and E. Mun, *Anisotropic magnetic property of single crystals RV_6Sn_6 ($R = Y, Gd-Tm, Lu$)*, Phys. Rev. Mater. **6**, 083401 (2022).
- [33] E. Rosenberg, J. M. DeStefano, Y. Guo, J. S. Oh, M. Hashimoto, D. Lu, R. J. Birgeneau, Y. Lee, L. Ke, M. Yi, and J.-H. Chu, *Uniaxial ferromagnetism in the kagome metal TbV_6Sn_6* , Phys. Rev. B **106**, 115139 (2022).
- [34] X. Zhang, Z. Liu, Q. Cui, Q. Guo, N. Wang, L. Shi, H. Zhang, W. Wang, X. Dong, J. Sun, Z. Dun, and J. Cheng, *Electronic and magnetic properties of intermetallic kagome magnets RV_6Sn_6 ($R = Tb-Tm$)*, Phys. Rev. Mater. **6**, 105001 (2022).
- [35] G. Pokharel, B. R. Ortiz, J. Chamorro, P. Sarte, L. Kautzsch, G. Wu, J. Ruff, and S. D. Wilson, *Highly anisotropic magnetism in the vanadium-based kagome metal TbV_6Sn_6* , Phys. Rev. Mater. **6**, 104202 (2022).
- [36] See Supplemental Material, which includes Refs. [37–55], for the details of crystal growth and characterization, photoemission measurements, electrical resistivity and magnetization measurements, specific-heat measurements, high-pressure measurements, and theoretical calculations, as well as other supporting data and discussion.
- [37] K. Koepnick and H. Eschrig, *Full-potential nonorthogonal local-orbital minimum-basis band-structure scheme*, Phys. Rev. B **59**, 1743 (1999).
- [38] J. P. Perdew and Y. Wang, *Accurate and simple analytic representation of the electron-gas correlation energy*, Phys. Rev. B **45**, 13244 (1992).
- [39] J. P. Perdew, K. Burke, and M. Ernzerhof, *Generalized gradient approximation made simple*, Phys. Rev. Lett. **77**, 3865 (1996).
- [40] D. Y. Usachov, D. Glazkova, A. V. Tarasov, S. Schulz, G. Poelchen, K. A. Bokai, O. Y. Vilkov, P. Dudin, K. Kummer, K. Kliemt, C. Krellner, and D. V. Vyalikh, *Estimating the orientation of 4f magnetic moments by classical photoemission*, J. Phys. Chem. Lett. **13**, 7861 (2022).

- [41] D. Y. Usachov, A. V. Tarasov, D. Glazkova, M. Mende, S. Schulz, G. Poelchen, A. V. Fedorov, O. Y. Vilkov, K. A. Bokai, V. S. Stolyarov, K. Kliemt, C. Krellner, and D. V. Vyalikh, *Insight into the temperature-dependent canting of 4f magnetic moments from 4f photoemission*, J. Phys. Chem. Lett. **14**, 5537 (2023).
- [42] K. Kummer, Y. Kucherenko, S. Danzenbächer, C. Krellner, C. Geibel, M. G. Holder, L. V. Bekenov, T. Muro, Y. Kato, T. Kinoshita, S. Huotari, L. Simonelli, S. L. Molodtsov, C. Laubschat, and D. V. Vyalikh, *Intermediate valence in Yb compounds probed by 4f photoemission and resonant inelastic x-ray scattering*, Phys. Rev. B **84**, 245114 (2011).
- [43] M. Güttler, K. Kummer, K. Kliemt, C. Krellner, S. Seiro, C. Geibel, C. Laubschat, Y. Kubo, Y. Sakurai, D. V. Vyalikh, and A. Koizumi, *Visualizing the Kondo lattice crossover in YbRh₂Si₂ with Compton scattering*, Phys. Rev. B **103**, 115126 (2021).
- [44] Q. Y. Chen *et al.*, *Direct observation of how the heavy-fermion state develops in CeCoIn₅*, Phys. Rev. B **96**, 045107 (2017).
- [45] S. Jang, J. D. Denlinger, J. W. Allen, V. S. Zapf, M. B. Maple, J. N. Kim, B. G. Jang, and J. H. Shim, *Evolution of the Kondo lattice electronic structure above the transport coherence temperature*, Proc. Natl. Acad. Sci. U.S.A. **117**, 23467 (2020).
- [46] A. Damascelli, Z. Hussain, and Z.-X. Shen, *Angle-resolved photoemission studies of the cuprate superconductors*, Rev. Mod. Phys. **75**, 473 (2003).
- [47] L. Li, S. Chi, W. Ma, K. Guo, G. Xu, and S. Jia, *Enhanced anomalous Hall effect in kagome magnet YbMn₆Sn₆ with intermediate-valence ytterbium*, Chin. Phys. B **33**, 057501 (2024).
- [48] E. Bauer, E. Gratz, R. Hauser, L. Tuan, A. Galatanu, A. Kottar, H. Michor, W. Perthold, G. Hilscher, T. Kagayama, G. Oomi, N. Ichimiya, and S. Endo, *Pressure- and field-dependent behavior of YbCu₄Au*, Phys. Rev. B **50**, 9300 (1994).
- [49] L. Spendeler, D. Jaccard, J. Sierro, M. François, A. Stepanov, and J. Voiron, *Resistivity and thermoelectric power of YbCu_{4.5} under very high pressure*, J. Low Temp. Phys. **94**, 585 (1994).
- [50] F. Steglich, J. Arndt, O. Stockert, S. Friedemann, M. Brando, C. Klingner, C. Krellner, C. Geibel, S. Wirth, S. Kirchner, and Q. Si, *Magnetism, f-electron localization and superconductivity in 122-type heavy-fermion metals*, J. Phys.: Condens. Matter **24**, 294201 (2012).
- [51] P. Ghaemi, T. Senthil, and P. Coleman, *Angle-dependent quasi-particle weights in correlated metals*, Phys. Rev. B **77**, 245108 (2008).
- [52] M. Dzero, J. Xia, V. Galitski, and P. Coleman, *Topological Kondo insulators*, Annu. Rev. Condens. Matter Phys. **7**, 249 (2016).
- [53] H.-H. Lai, S. E. Grefe, S. Paschen, and Q. Si, *Weyl-Kondo semimetal in heavy-fermion systems*, Proc. Natl. Acad. Sci. U.S.A. **115**, 93 (2018).
- [54] M. Keßler and R. Eder, *Magnetic phases of the triangular Kondo lattice*, Phys. Rev. B **102**, 235125 (2020).
- [55] H. J. Elmers *et al.*, *Chirality in the kagome metal CsV₃Sb₅*, Phys. Rev. Lett. **134**, 096401 (2025).
- [56] D. C. Fredrickson, S. Lidin, G. Venturini, B. Malaman, and J. Christensen, *Origins of superstructure ordering and incommensurability in stuffed CoSn-type phases*, J. Am. Chem. Soc. **130**, 8195 (2008).
- [57] C. M. Varma, *Mixed-valence compounds*, Rev. Mod. Phys. **48**, 219 (1976).
- [58] L. I. Johansson, J. W. Allen, I. Lindau, M. H. Hecht, and S. B. M. Hagström, *Photoemission from Yb: Valence-change-induced Fano resonance*, Phys. Rev. B **21**, 1408 (1980).
- [59] K. Kummer, S. Patil, A. Chikina, M. Güttler, M. Höppner, A. Generalov, S. Danzenbächer, S. Seiro, A. Hannaske, C. Krellner, Y. Kucherenko, M. Shi, M. Radovic, E. Rienks, G. Zwicknagl, K. Matho, J. W. Allen, C. Laubschat, C. Geibel, and D. V. Vyalikh, *Temperature-independent Fermi surface in the Kondo lattice YbRh₂Si₂*, Phys. Rev. X **5**, 011028 (2015).
- [60] M. Okusawa, E. Weschke, R. Meier, G. Kaindl, T. Ishii, N. Sato, and T. Komatsubara, *Temperature dependence of the valence-band photoemission spectra in YbInCu₄*, J. Electron Spectrosc. Relat. Phenom. **78**, 139 (1996).
- [61] H. Sato, K. Yoshikawa, K. Hiraoka, M. Arita, K. Fujimoto, K. Kojima, T. Muro, Y. Saitoh, A. Sekiyama, S. Suga, and M. Taniguchi, *Soft-x-ray high-resolution photoemission study on the valence transitions in YbInCu₄*, Phys. Rev. B **69**, 165101 (2004).
- [62] S. Chatterjee, J. P. Ruf, H. I. Wei, K. D. Finkelstein, D. G. Schlom, and K. M. Shen, *Lifshitz transition from valence fluctuations in YbAl₃*, Nat. Commun. **8**, 852 (2017).
- [63] A. Yatskar, C. H. Mielke, P. C. Canfield, A. H. Lacerda, and W. P. Beyermann, *Magnetotransport in the heavy-fermion system YbNi₂B₂C*, Phys. Rev. B **60**, 8012 (1999).
- [64] S. L. Bud'ko, E. Morosan, and P. C. Canfield, *Magnetic field induced non-Fermi-liquid behavior in YbAgGe single crystals*, Phys. Rev. B **69**, 014415 (2004).
- [65] E. D. Mun, S. L. Bud'ko, C. Martin, H. Kim, M. A. Tanatar, J.-H. Park, T. Murphy, G. M. Schmiedeshoff, N. Dilley, R. Prozorov, and P. C. Canfield, *Magnetic-field-tuned quantum criticality of the heavy-fermion system YbPtBi*, Phys. Rev. B **87**, 075120 (2013).
- [66] M. Kang, L. Ye, S. Fang, J.-S. You, A. Levitan, M. Han, J. I. Facio, C. Jozwiak, A. Bostwick, E. Rotenberg, M. K. Chan, R. D. McDonald, D. Graf, K. Kaznatcheev, E. Vescovo, D. C. Bell, E. Kaxiras, J. van den Brink, M. Richter, M. P. Ghimire, J. G. Checkelsky, and R. Comin, *Dirac fermions and flat bands in the ideal kagome metal FeSn*, Nat. Mater. **19**, 163 (2020).
- [67] S. Danzenbächer, Y. Kucherenko, D. V. Vyalikh, M. Holder, C. Laubschat, A. N. Yaresko, C. Krellner, Z. Hossain, C. Geibel, X. J. Zhou, W. L. Yang, N. Mannella, Z. Hussain, Z.-X. Shen, M. Shi, L. Patthey, and S. L. Molodtsov, *Momentum dependence of 4f hybridization in heavy-fermion compounds: Angle-resolved photoemission study of YbIr₂Si₂ and YbRh₂Si₂*, Phys. Rev. B **75**, 045109 (2007).
- [68] S. Peng, Y. Han, G. Pokharel, J. Shen, Z. Li, M. Hashimoto, D. Lu, B. R. Ortiz, Y. Luo, H. Li, M. Guo, B. Wang, S. Cui, Z. Sun, Z. Qiao, S. D. Wilson, and J. He, *Realizing kagome band structure in two-dimensional kagome surface states of RV₆Sn₆ (R = Gd, Ho)*, Phys. Rev. Lett. **127**, 266401 (2021).
- [69] D. D. Sante, C. Bigi, P. Eck, S. Enzner, A. Consiglio, G. Pokharel, P. Carrara, P. Orgiani, V. Polewczyk, J. Fujii, P. D. C. King, I. Vobornik, G. Rossi, I. Zeljkovic, S. D. Wilson, R. Thomale, G. Sangiovanni, G. Panaccione, and F. Mazzola, *Flat band separation and robust spin Berry curvature in bilayer kagome metals*, Nat. Phys. **19**, 1135 (2023).
- [70] Y. Hu, X. Wu, Y. Yang, S. Gao, N. C. Plumb, A. P. Schnyder, W. Xie, J. Ma, and M. Shi, *Tunable topological Dirac surface states and van Hove singularities in kagome metal GdV₆Sn₆*, Sci. Adv. **8**, eadd2024 (2022).
- [71] V. N. Strocov, *Intrinsic accuracy in 3-dimensional photoemission band mapping*, J. Electron Spectrosc. Relat. Phenom. **130**, 65 (2003).
- [72] H. Tan and B. H. Yan, *Abundant lattice instability in kagome metal ScV₆Sn₆*, Phys. Rev. Lett. **130**, 266402 (2023).
- [73] K. Kummer, D. V. Vyalikh, L. Rettig, R. Cortés, Y. Kucherenko, C. Krellner, C. Geibel, U. Bovensiepen, M. Wolf,

- and S. L. Molodtsov, *Ultrafast quasiparticle dynamics in the heavy-fermion compound YbRh₂Si₂*, Phys. Rev. B **86**, 085139 (2012).
- [74] P. Fulde and M. Loewenhaupt, *Magnetic excitations in crystal-field split 4f systems*, Adv. Phys. **34**, 589 (1985).
- [75] E. Schuberth, M. Tippmann, L. Steinke, S. Lausberg, A. Steppke, M. Brando, C. Krellner, C. Geibel, R. Yu, Q. Si, and F. Steglich, *Emergence of superconductivity in the canonical heavy-electron metal YbRh₂Si₂*, Science **351**, 485 (2016).
- [76] L. Eichenberger, G. Venturini, B. Malaman, L. Nataf, F. Baudalet, and T. Mazet, *Commensurate-incommensurate magnetic phase transition in the new Yb_{1-x}Lu_xMn₆Sn₆ compounds*, J. Alloys Compd. **695**, 286 (2017).
- [77] A. Maignette, A. Vernière, G. Venturini, L. Eichenberger, B. Malaman, and T. Mazet, *Crystal and magnetic properties of YbMn_{6-y}Fe_ySn₆ ($y \leq 1$)*, J. Magn. Magn. Mater. **458**, 19 (2018).
- [78] S. Doniach, *The Kondo lattice and weak antiferromagnetism*, Physica (Amsterdam) **91B+C**, 231 (1977).
- [79] A. L. Cornelius, J. S. Schilling, D. Mandrus, and J. D. Thompson, *Anomalous hydrostatic pressure dependence of the Curie temperature of the Kondo-lattice compound YbNiSn to 38 GPa*, Phys. Rev. B **52**, R15699(R) (1995).